



1 **High-resolution automated detection of headwater streambeds for large watersheds**

2 **Francis Lessard^{1,2,3}, Naïm Perreault^{1,2}, Sylvain Jutras^{1,2,3}**

3 ¹ Department of Wood and Forest Science, Université Laval, 2405 rue de la Terrasse, G1V

4 0A6, Québec, QC, Canada

5 ² Centre d'étude de la forêt, Université Laval, 2405 rue de la Terrasse, G1V 0A6, Québec,

6 QC, Canada

7 ³ CentrEau - Water Research Centre, Université Laval, 1065 avenue de la Médecine, G1V

8 0A6, Québec, QC, Canada

9

10 **Corresponding author:** Francis Lessard, francis.lessard.3@ulaval.ca

11 **Present address:** Pavillon Abitibi-Price, 2405 rue de la Terrasse, G1V 0A6, Québec, QC,

12 Canada

13

14 **Keywords:** LiDAR, Streambed, Headwater stream, Remote sensing



15 **Abstract:** Streams are defined by the presence of a streambed, which is a linear
16 depression where water flows between discernible banks. The upstream
17 boundary of a stream is called a channel head. Headwater streams, which are
18 small streams at the top of a watershed, account for the majority of the total
19 length of streams, yet their exact locations are still not well known. For years,
20 many algorithms were used to produce hydrographic networks that represent
21 headwater streams with varying degrees of accuracy. Although digital
22 elevation models derived from LiDAR have significantly improved headwater
23 stream detection, the performance of the algorithms with different geomorphic
24 characteristics remains unclear. Here, we address this issue by testing different
25 combinations of algorithms using classification trees. Homogeneous
26 hydrological processes were identified through hydrological classification. The
27 results showed that in shallow soil that mainly consists of till deposits, the
28 algorithms that recreate the surface runoff process provide the best explanation
29 for the presence of a streambed. In contrast, streambeds in thick soil with high
30 infiltration rates were primarily explained by a small scale incision algorithm.
31 Furthermore, the use of an iterative process that recreates water diffusion made
32 it possible to more accurately detect streambeds than other methods tested,
33 regardless of the hydrological classification. The method developed in this
34 paper shows the importance of considering hydrological processes when
35 aiming to identify headwater streams.

36 223 words

37



38 **1. Introduction**

39 Streams are characterized by the presence of natural linear depressions, called streambeds.
40 Streambeds, which are mostly formed by fluvial processes, consist of a bed floor and banks,
41 and are identified morphologically. The upstream location of a streambed is generally
42 recognized as being the beginning of a stream and is referred as the channel head. At times,
43 streambeds can be discontinuous or diffuse, leading to subjective identification of
44 streambeds in the field and influence the determined location of the surveyed channel head
45 (Dietrich and Dunne, 1993; Wohl, 2018). On a large scale, headwater streams are
46 extremely important to maintain natural hydrological processes. Indeed, they are
47 representing about two-thirds of the total length of streams in a large watershed (Leopold
48 et al., 1964). Because they have varied ecosystems that include ecotones, headwater
49 streams support rich and diverse fauna and flora (Meyer et al., 2007). In addition,
50 headwater streams provide many ecological services to humans, including good quality
51 drinking water (Alexander et al., 2007; Freeman et al., 2007) and flood control (St-Hilaire
52 et al., 2016). Creed et al. (2017) estimated that for 2.9 million km of headwater streams in
53 the United States, 15.7 trillion US \$ in ecological services are provided annually.
54 Cartographic information on headwater streams at national or provincial scales are largely
55 derived from photointerpretation of stereoscopic aerial photography. This is the main
56 method used for the Géobase du réseau hydrographique du Québec (GRHQ) in Quebec
57 province, Canada. This geodatabase combines and standardizes several sources of
58 hydrographic data, covering an area of 154 million hectares and representing millions of
59 hydrographic features identified from aerial photos. Unfortunately, this method
60 underestimates the true length of streams and is especially inaccurate when identifying



61 where streams begin and where they become permanent. Streambeds are often
62 imperceptible on stereoscopic images where only the wide valleys are evident
63 (Montgomery and Dietrich, 1994).

64 Other methods based on a digital elevation model (DEM) have been used for several years
65 to detect streams. These methods, used to produce hydrographic networks, can be divided
66 into two main categories: channel initiation and valley recognition (Lindsay, 2006). The
67 channel initiation method can be used to identify the potential locations of streambeds by
68 thresholding a flow accumulation raster by a minimum drainage area (Band, 1986; Fairfield
69 and Leymarie, 1991; Jenson and Dominique, 1988; O'Callaghan and Mark, 1984). Valley
70 recognition can be used to detect streambeds locally through a moving window that
71 identifies specific pattern depending on the algorithm used (Passalacqua et al., 2012;
72 Peucker and Douglas, 1975; Tribe, 1992). These methods have been widely used with
73 coarse resolution DEMs (greater than 10 m) that have generally been derived from aerial
74 photos.

75 High resolution geospatial data from LiDAR technology allows for more accurate detection
76 of headwater streams. These data have recently been made available over large areas,
77 providing topographic data on the microtopography under the forest canopy and allowing
78 the creation of DEMs with unprecedented accuracy (Wulder et al., 2008). The
79 hydrographic networks generated with these new DEMs are much more accurate than those
80 derived from photointerpretation or those produced from DEMs with a coarser resolution
81 (Goulden et al., 2014). These DEMs allow for the subdivision of a larger number of small,
82 previously undetected watersheds, thus generating multiple headwater streams, and
83 consequently, many branches. Various authors have attempted to use these DEMs to



84 improve the accuracy of hydrographic networks and the position of channel heads. LiDAR-
85 derived DEMs have been used to detect streams both locally (Cho et al., 2011; James et
86 al., 2007) and through channel initiation using a drainage area threshold (Murphy et al.,
87 2008; Persendt and Gomez, 2016). Other authors have attempted to include the slope to a
88 flow accumulation raster in order to produce more explicit models (Elmore et al., 2013;
89 Henkle et al., 2011; James et al., 2010; Montgomery and Foufoula-Georgiou, 1993). While
90 these methods are more representative of the local impact of water, they still ignore the
91 heterogeneity of an area and the many other elements that affect bed formation. Among
92 other things, some authors noted the sensitivity of local flow direction to the elevation error
93 of the DEM (Hengl et al., 2010; O’Neil and Shortridge, 2013; Schwanghart and Heckmann,
94 2012). DEMs derived from LiDAR data were also used to quantify the variability of
95 permanent stream flow lengths, although those studies did not specify where the streambed
96 begins (Jensen et al., 2018, 2019; Van Meerveld et al., 2019). To the best of our knowledge,
97 no study has addressed streambed detection using LiDAR data while considering both
98 channel initiation and valley recognition methods (Heine et al., 2004) on a heterogeneous
99 territory at the geomorphological level (Wu et al., 2021). Also, no study uses such a large
100 validation database from real observations acquired in the field.

101 The main objective of our study is to detect headwater streambeds at a provincial scale.
102 Our method overcomes the many challenges that have limited this information in the past.
103 These challenges include highly heterogeneous geomorphological characteristics (such as
104 surface deposits) and strong anthropization of the land.



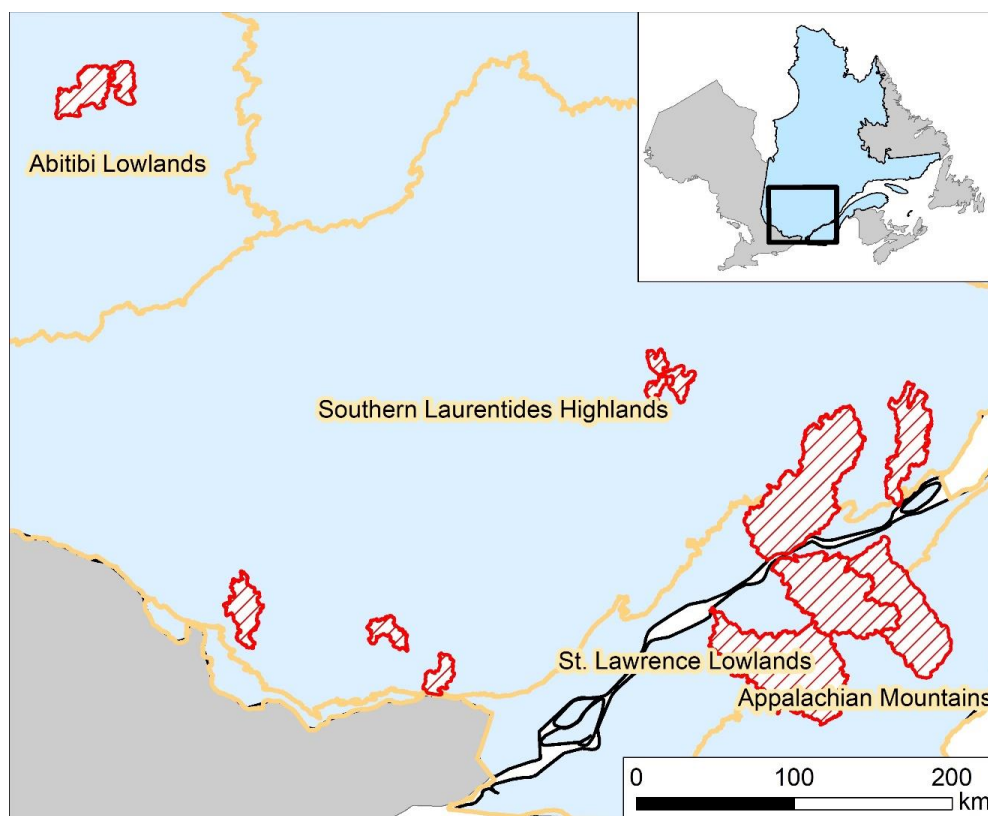
105 **2. Study areas**

106 The study areas were located in the Appalachian Mountains, St. Lawrence Lowlands,
107 Southern Laurentides Highlands and Abitibi Lowlands natural provinces, according to the
108 Quebec Ecological Reference Framework (Fig. 1). This reference framework divides the
109 territory of Quebec into spatially homogeneous units at various, intertwined levels. The
110 different levels describe homogeneous units in terms of landform, spatial organization and
111 hydrographic network configuration (Direction de l'expertise en biodiversité, 2018). The
112 diversity of the natural provinces thus selected provides a general description of the
113 headwater streams in Quebec. These natural provinces have distinct hydrological
114 processes.

115 The Southern Laurentides Highlands is mostly covered by till, the most widespread surface
116 deposit in the province of Quebec (Blouin and Berger, 2004; Gosselin, 2002). This natural
117 province is mountainous, with altitudes varying from 200 to 1200 m. The bedrock mainly
118 consists of gneiss. Surface deposits are generally thin on summits and steep slopes and
119 thicker on valley bottoms and gentle slopes. The land in the Southern Laurentides
120 Highlands is largely forested. In the Appalachian Mountains, the surface deposits are
121 somewhat similar in distribution to those in the Southern Laurentides Highlands, although
122 they are thicker in certain areas. However, the bedrock in the Appalachian Mountains is
123 sedimentary and therefore very different from the Southern Laurentides Highlands. The
124 altitude here varies from 0 to 1200 m. Unlike the Southern Laurentides Highlands, there is
125 high anthropization of this natural province due to urbanization and agriculture (Gosselin,
126 2005a). In the St. Lawrence Lowlands, agricultural activity is also widespread. The surface
127 deposits in this region are highly heterogeneous and are mainly derived from marine and



128 glaciolacustrine geomorphic processes. These processes lead to thick soils of sorted
129 material, including clay and sand. These, in turn, create deposits that range from
130 impermeable to very permeable. In addition to clay and sand, organic deposits are also
131 present. The elevation of the St. Lawrence Lowlands is generally less than 100 m, as it was
132 formed from the Champlain Sea during deglaciation (Gosselin, 2005b). In the Abitibi
133 Lowlands, the surface deposits are rather thick and consist of silt and clay. These deposits
134 were produced by marine and lacustrine invasions and are conducive to the formation of
135 large peatlands. Therefore, the area is relatively flat with altitudes varying from 0 to 350
136 m. Where present, the bedrock is made of basalt and gneiss (Blouin and Berger, 2002).
137 Precipitation is not seasonal, but rather constant throughout the year in all study areas.
138 Precipitation amounts are quite homogeneous and range from 900 mm/year to 1100
139 mm/year, except in Southern Laurentides Highlands where it can reach 1450 mm/year.
140 Approximately 20 % of the precipitation falls as snow during the cold season, except in the
141 coldest regions such as the Abitibi Lowlands and the higher altitude areas of the Southern
142 Laurentides Highlands where the proportion of snow can reach 30%. Indeed, the average
143 annual temperature of all the study areas is 3° C to 5° C, except for these two regions where
144 it is 0° C (MELCC, 2022).



145

146 **Figure 1** : Study areas in the Appalachian Mountains, St. Lawrence Lowlands, Southern
147 Laurentides Highlands and Abitibi Lowlands natural provinces. [Color is not required
148 for this figure. Single column fitting figure.]

149

150 3. Methods

151 3.1. Field surveys

152 Field based data collection is essential to fully understand stream flow patterns. Field
153 surveys were conducted from 2017 to 2021 during summer periods using an EOS GNSS
154 Arrow 100 sub-meter precision GPS. The horizontal accuracy of these devices is
155 ± 0.6 m in open areas and ± 1.2 m in forested areas (Estrada, 2017). These devices were



156 connected to rugged cell phones in order to use the ArcGIS Field Maps application to
157 integrate data collection forms as well as relevant background maps.

158 The positions of streams were recorded from downstream at drainage area generally under
159 1000 ha to upstream until the streambed completely disappeared. The flow regime, the
160 width of the streambed, the extent of the water occupation in the streambed and the
161 presence or the absence of a water flow were collected along the stream path to establish a
162 high level of understanding. A position was taken on the streams every 50 m or so where
163 a streambed was present, i.e. where the stream had a bed floor and banks formed by a
164 fluvial process. Other positions were also taken to identify where there was no streambed.
165 These information were essential for consistent calibration and validation of streambeds.
166 To ensure consistent data collection, a 50 m x 50 m grid was used to determine which areas
167 should be fully surveyed. These areas were mostly located at headwater streams in order
168 to be able to include channel heads. This procedure was essential to properly assess the
169 upstream boundary of the headwater streams and precisely record where the streambeds
170 begin, where they flow from the watershed to the permanent stream, and where they are
171 absent.

172 3.2. *Variables used for analysis*

173 The geomatic manipulations were mainly performed with the ArcGIS Desktop 10.7
174 software package, including the Spatial Analyst and 3D Analysis extensions. The open
175 source SAGA-GIS (Conrad et al., 2015) and WhiteboxTools (Lindsay, 2016a) software's
176 were also used.

177 The variables used for analysis were produced from 1 m resolution DEMs of the different
178 areas. These were generated from LiDAR data from the MFFP (Ministère des Forêts, de la



179 Faune et des Parcs), with a density of around 2.5 points/m². LiDAR acquisitions were
180 conducted from 2016 to 2019 (Leboeuf and Pomerleau, 2015), with the exception of a few
181 areas. The road network was carefully examined in order to include and burn all culverts
182 that could affect the flow direction (Lessard et al., 2023). Hydrographic networks are
183 greatly affected by deviations caused by the embankment of the roads. This type of
184 anthropic influence must therefore be minimized in order to generate coherent flow
185 direction (Li et al., 2013). Furthermore, the use of a breaching algorithm allowed to
186 generate hydrologically coherent DEMs prior to hydrographic modeling (Lindsay, 2016b;
187 Lindsay and Dhun, 2015). Physiographic factors must also be considered during the
188 modeling process as they significantly influence the location of channel heads and the flow
189 regime along streams. On the local scale, where the precipitation regime is uniform (Tucker
190 and Slingerland, 1996), slope, hydraulic force and sediment cohesion generally dictates
191 streambed formation (Dietrich and Dunne, 1978). The influence of these factors is variable
192 depending on the type of surface deposit (Dietrich and Dunne, 1993; Dunne and Black,
193 1970; Montgomery and Dietrich, 1994).

194 Surface deposits can be used to assess which processes are involved in the formation of a
195 streambed. Indeed, there are two major types of formation processes. The first type
196 involves surface processes, which occurs when soil that has low permeability is exposed
197 to rainfall amounts that exceed the infiltration capacity of the ground, causing surface
198 runoff (Horton, 1945). Then, when the power of the water exceeds the cohesion of the
199 sediments, usually in concavities, a streambed forms (Dietrich and Dunne, 1978). The
200 second type involves subsurface processes that occur when the surface deposits are thick
201 and infiltrative. Water vertically infiltrates into the ground and eventually reaches



202 saturation at a junction with the bedrock or an inferior and less infiltrating deposit. Then,
203 lateral movement of the groundwater occurs. Water emerges from the ground when there
204 is a change in slope or soil permeability. Streambeds formed in this way tend to be heavily
205 incised, with flow regimes that are more stable than those formed through surface
206 processes. Thus, the hydrological response of the streams from subsurface processes is
207 slightly affected by the intensity of rainfall (Dunne and Black, 1970; Jensen et al., 2019;
208 Wohl, 2018). Furthermore, it should be noted that there is a gradient between these two
209 processes for each stream. In order to properly detect streambeds, it is essential to
210 distinguish these processes through hydrological classification according to surface deposit
211 type and land use.

212 Surface deposit mapping has been standardized across the province, including our study
213 area. Information was collected through photointerpretation conducted several years ago.
214 Since photointerpretation was mainly used to distinguish forest structures and land use, the
215 true boundaries of the surface deposits are imprecise, in some cases. Surface deposit
216 boundaries in agricultural areas are more accurate than those in forested areas because no
217 other information was mapped during the process. Regardless of these drawbacks,
218 standardized mapping provides a rough description of the nature and thickness of surface
219 deposits.

220 Spatially heterogeneous surface deposits in Quebec have been classified into three
221 categories and are described in Table 1 (Saucier et al., 1994). The purpose of this
222 classification step is to differentiate the two types of hydrological processes for headwater
223 stream formation that were previously described (Dietrich and Dunne, 1993; Lessard,
224 2020). These classifications consider the infiltration capacity and the water storage



225 capacity of the ground (Dunne and Black, 1970). The two main variables considered were
226 the potential thickness and the granulometry of the surface deposits (Dietrich and Dunne,
227 1993; Wohl, 2018).

228

229 **Table 1** : Hydrological classification according to surface deposit types and land use

Hydrological class	Surface deposits and land use involved
Shallow soil	Glacial deposits without morphology such as till, frequent rock outcrops
Thick soil with high infiltration rate (including anthropogenic land use)	Glacial deposits with morphology such as moraines, glaciofluvial deposits, fluvial deposits, coarse lacustrine and marine deposits, slope deposits and eolian deposits; Anthropogenic land use were included in this class (Treeless areas including agricultural fields, roads, urbanized areas and powerlines)
Thick soil with low infiltration rate	Lacustrine and fine marine deposits, organic deposits

230

231 The first analysis variable, called 'D8', refers to the D8 flow accumulation (O'Callaghan
232 and Mark, 1984) produced with a 1 m resolution DEM. This variable was selected as it is
233 the most common algorithm used to produce hydrographic networks. For meaningful
234 correspondence analysis between this variable and field surveyed streams, the flow
235 accumulation raster was aggregated at 3 m resolution according to the maximum value.



236 Then, a maximum focal statistic of two pixels was applied. The purpose of this treatment
237 was to ensure a 6 m analysis distance between the D8 and the edge of a real stream,
238 represented in the database by a geospatial line. This prevents the omission error from
239 being overestimated.

240 The second analysis variable uses the D8 flow accumulation algorithm while considering
241 flow direction error due to the elevation uncertainty of the DEM (Hengl et al., 2010;
242 O’Callaghan and Mark, 1984). This variable, called ‘PROB’, quantifies the uncertainty
243 associated with the position of the drainage network. The elevation error in the DEM is
244 directly related to the uncertainty of the LiDAR data (Wechsler, 2007) and impacts the
245 position of the hydrographic network (Lindsay, 2006). This type of error is affected by the
246 landform, and mainly occurs on gentle slopes and slightly convex terrain (Hengl et al.,
247 2010). Since this type of error is inherent to the shape of the land, it is not affected by the
248 size of the drainage area implied. The iterative method described in Hengl et al. (2010) was
249 reproduced in order to create the PROB variable. The method is based on repeatedly
250 computing a flow accumulation raster from an initial DEM and several altered versions of
251 the DEM. These altered versions are created by adding random elevation errors to the initial
252 DEM in order to reproduce the elevation errors from the LiDAR data. The elevation errors
253 therefore had a standard deviation of 0.08 m, randomly distributed over the DEM. A focal
254 statistic of 3 m was used on the error raster to ensure the spatial autocorrelation of errors.
255 Based on the convergence observed by (Lindsay, 2006), 50 iterations were carried out.
256 Then, each of the flow accumulation rasters were thresholded to a 1.5 ha drainage area to
257 sum the resulting binary stream network, where a value of 1 indicated the presence of a
258 streambed and a 0 indicated the absence of a streambed. The matrix of the cumulative value



259 was then normalized as a percentage to be used as an analysis variable. This PROB variable
260 revealed the diffusion process of the water in hillsides, where the slope is relatively
261 uniform. The PROB variable was produced with a 3 m resolution DEM from a 1 m
262 resolution DEM that was aggregated using the mean values. An average flow accumulation
263 raster that corresponded to the average of the 50 flow accumulations raster without
264 thresholding was also produced. This raster was used to create the analysis database and to
265 calculate the drainage area of the channel heads. To ensure a 6 m analysis distance as well
266 as the D8 variable, a maximum focal statistic of two cells was performed before summing
267 or averaging the iterated raster.

268 The third variable used for analysis is morphometric and allows for the complementary
269 detection of headwater streams (Lindsay, 2006; Tribe, 1992). The morphometric algorithm
270 used was the topographic position index, referred to as 'TPI'. This algorithm allowed for
271 the local detection of small incisions that might represent streambeds (Tribe, 1992). The
272 scale at which this variable is calculated strongly influences the morphometric feature that
273 is identified. When the scale is large, the variable will tend to identify valleys, while it
274 tends towards streambeds when the scale is small (Montgomery and Dietrich, 1992, 1994).
275 For the purposes of this paper, a relatively small scale of 6 to 30 m was used. This scale is
276 consistent with the width of the majority of inventoried streambeds. The DEM used to
277 calculate this variable had a resolution of 2 m and was derived from aggregating a 1 m
278 resolution DEM with the minimum values. The tool named 'Topographic Position Index'
279 in SAGA-GIS software was used to produce this variable (Guisan et al., 1999; Weiss,
280 2001). The TPI variable has not been normalized to keep the homogeneity of the values
281 between the different study areas.



282 3.3. *Analysis database*

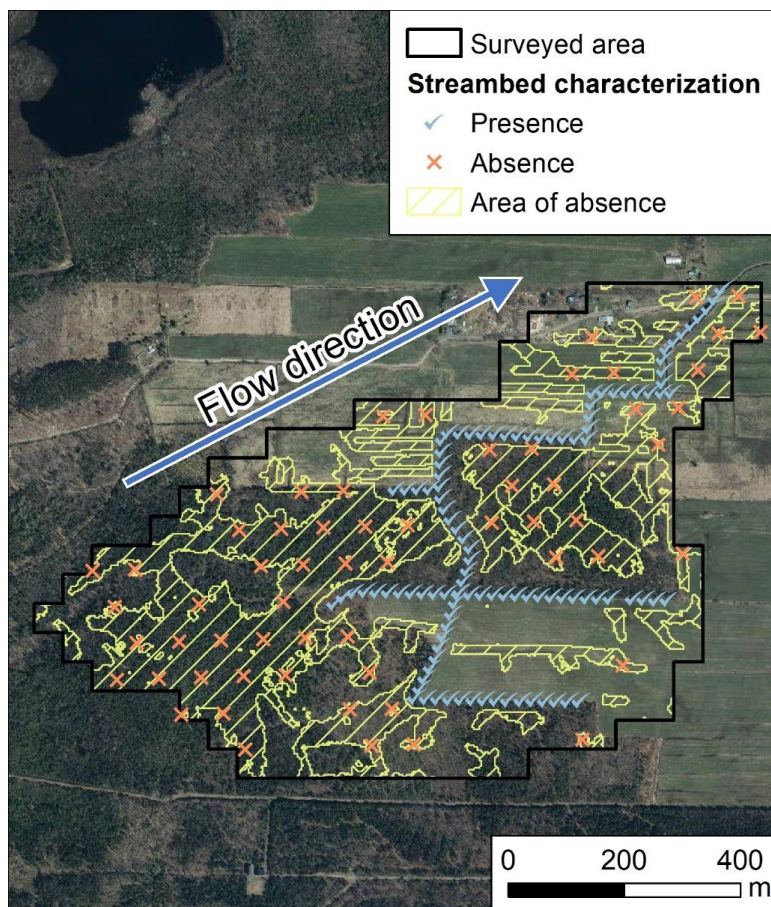
283 In order to perform the subsequent analyses, all actual streambeds were vectorized and geo-
284 interpreted according to the stream positions recorded in the field. It should be noted that
285 information on the flow regime was not used in this database. Instead, the presence of a
286 streambed was used to describe the presence or absence of a stream. Although some beds
287 have been excavated and channelized, particularly in anthropogenic lands, a bed was
288 considered to be present when natural fluvial processes allow it to be maintained. The
289 geospatial lines indicating the exact location of the streambeds were complemented by a
290 50 m x 50 m grid to represent the complete surveyed area. Thus, areas without a geospatial
291 line have been assumed to not contain streambeds.

292 Positions representing the presence of streams were systematically located every 20 m
293 along geospatial lines that described real streams. Then, positions representing the absence
294 of a streambed were located according to a sampling principle based on minimum flow
295 accumulation where it was still possible to observe the presence of a stream. First, within
296 the grid of the surveyed area, the average flow accumulation raster was thresholded at 0.11
297 ha. This threshold represents the lowest drainage area of a channel head according to
298 (Lessard, 2020). Then, the resulting raster was converted to a polygon. Following that step,
299 a 20 m buffer zone was removed around the geospatial lines that represent real streams.
300 Finally, absence positions were systematically located according to a hexagonal
301 distribution in the final resulting polygon. Thus, polygons identifying absence positions
302 were located only in areas with a minimum 1100 m² mean drainage area and a minimum
303 distance of 20 m from any real streams. The number of absence positions was equalized



304 with the number of presence positions for each natural region within the Quebec ecological
305 reference framework.

306 The analysis database was therefore composed of positions describing both the presence
307 and the absence of streambeds (Fig. 2). The values for the three variables described in the
308 previous section (D8, PROB and TPI) were extracted for all presence and absence
309 positions.



310

311 **Figure 2** : Analysis database of positions indicating the presence and absence of
312 streambeds (Aerial images from continuous imagery of the Government of Quebec;
313 MRNF). [Color is not required for this figure. Single column fitting figure.]



314

315 *3.4. Statistical analysis*

316 A total of nine logistic regression models were produced, one for each explanatory variable
317 and hydrologic class combination. Response variable was the presence (1) or the absence
318 (0) of a streambed. The area under the ROC (Receiver Operating Characteristic) curve was
319 used to evaluate model performance (Fawcett, 2006). The ROC curve plots the true positive
320 rate (1 minus omission) relative to the false positive rate (commission). This curve shows
321 the performance of a given variable by determining the Area Under the Curve (AUC) and
322 how the increase in the true positive rate will lead to an increase in the false positive rate.
323 A model with a high AUC will provide a better balance between these two measurements
324 and will produce better results. Thus, the AUC provides a measure of the ability of the
325 individual variables to detect a streambed.

326 Next, four streambed models were compared to each other. Detection performance was
327 calculated according to hydrological class and using Cohen's kappa, which is a measure of
328 agreement between the true positive rate and the false positive rate (Cohen, 1960).

329 The first model examined was the GRHQ. An analysis distance of 6 m was used in order
330 to compare properly the performance of the GRHQ with the other models. Two of the other
331 three models corresponded to two different thresholds that were applied to the D8 variable,
332 which is one of the most commonly used variables for generating stream networks. The
333 first threshold was the median of the average drainage area of the channel heads surveyed
334 in the field (referred to as Channel head). The second threshold was the one that maximized
335 Cohen's kappa for the variable D8 (referred to as Max Kappa). The last model that was
336 compared is based on a supervised classification approach. This approach groups
337 observations according to explanatory variables based on previously determined groups,



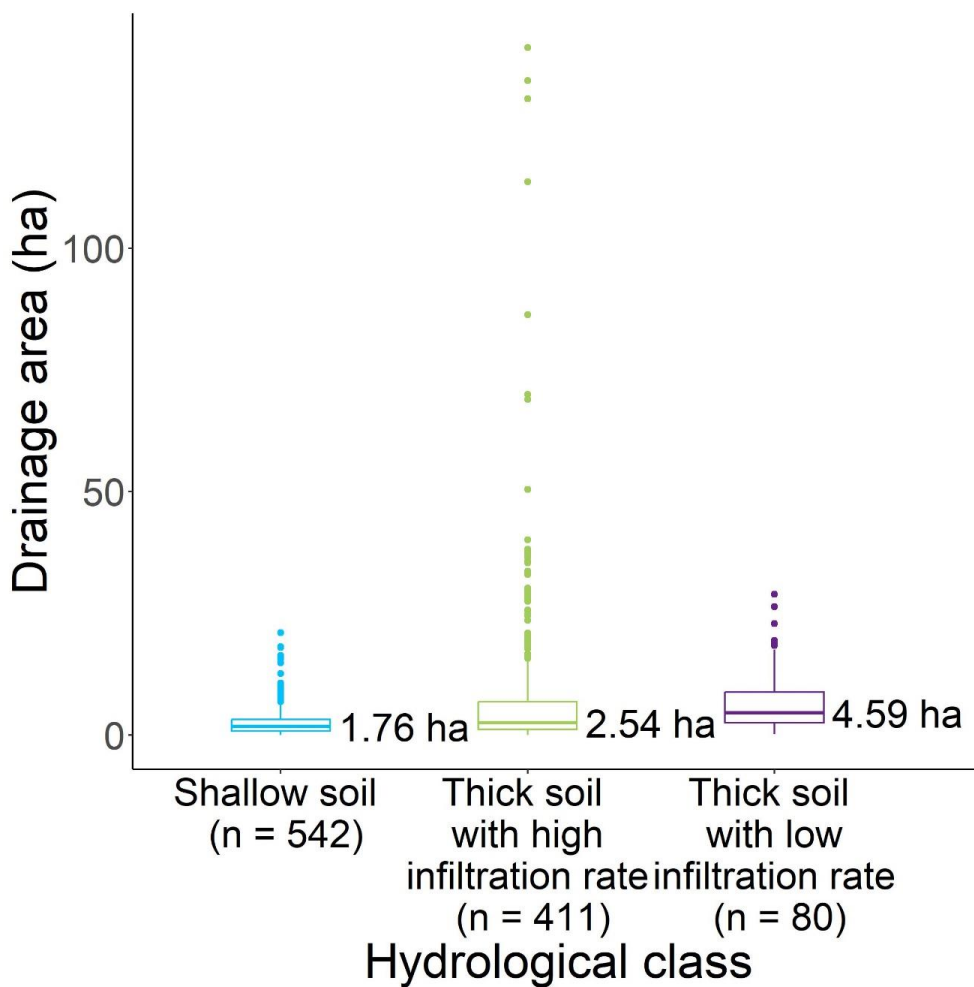
338 also known as the response variable. In this case, the response variable was the presence
339 or absence of a streambed. Classification And Regression Tree (CART) approach was used
340 because it is simple to apply over a large territory (Breiman et al., 1984). This model was
341 called CART. One tree was produced for each hydrologic class in order to describe the
342 formation of headwater streams from homogeneous hydrologic processes. Based on the
343 literature, different variables were used for each hydrological class. The PROB variable
344 was the only one that was used to detect streambeds in shallow soil, as the bedrock is
345 usually close to the surface of the ground and not very suitable for incisions (Jensen et al.,
346 2018). For the other two hydrological classes in thick soils, the TPI and PROB variables
347 were used. The surface deposits in these classes are not consolidated, allowing the ground
348 to be incised. This can then be detected by different morphometric indices (Montgomery
349 and Dietrich, 1994). The depth and number of branches in the classification trees have been
350 limited in order to prevent overfitting (Fürnkranz, 1997).

351

352 **4. Results**

353 A total of 464.7 km of streams were surveyed over a known territory of 161.5 km². The
354 positions for 1033 channel heads indicating the beginnings of streambeds were determined.
355 The average drainage areas of the channel head are presented in Fig. 3 using whisker boxes
356 according to hydrological class. Figure 3 shows that for shallow soil, the average drainage
357 area is less variable than for thick soils. For thick soils with low infiltration rates, the
358 average drainage area tends to be higher.

359



360

361 **Figure 3** : Distribution of mean drainage areas of channel heads according to hydrological
362 class. Median values are shown. [Color is not required for this figure. Single column
363 fitting figure.]

364

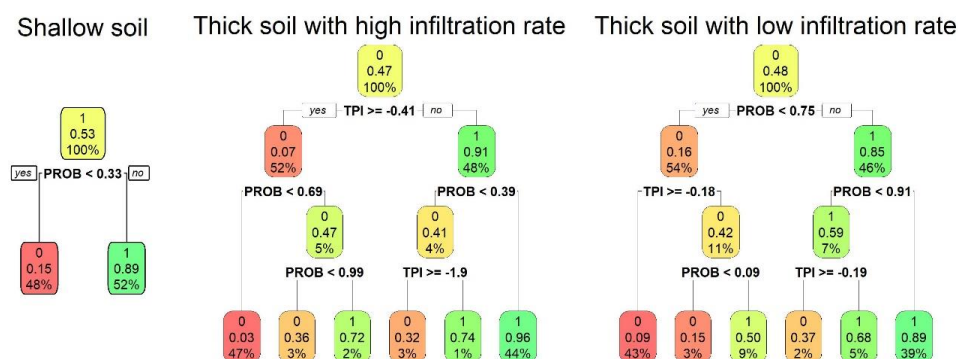
365 The analysis database contains a total of 40 354 positions describing streambeds (20 177
366 with streambeds present and 20 177 with streambeds absent) located in the entire surveyed
367 area. A correlation matrix between the analysis variables showed that PROB is negatively



368 correlated with TPI, with an R of -0.57. This variable therefore identifies where the water
 369 converges, which usually corresponds with the locations of incisions. The other variables
 370 were not correlated with each other.

371 Three classification trees according to hydrological class are presented in Fig. 4. The tree
 372 for shallow soil shows that when PROB exceeds a threshold of 0.33, a streambed is
 373 generally present. For thick soil with a high infiltration rate, the incision indicated by the
 374 TPI first explains the presence of a streambed. When the incision is greater or equal to -
 375 0.41, indicating a small incision, PROB must be very high in order to indicate the presence
 376 of a streambed, at 0.99. When there is a larger incision, a lower value for PROB can identify
 377 the presence of a streambed. Thus, when the ground is relatively well incised with a TPI
 378 value smaller than -0.41, PROB only needs to be higher than 0.39 to detect a streambed.
 379 In thick soil with a low infiltration rate, PROB provides the initial information regarding
 380 the presence or absence of a streambed. Depending on the different PROB thresholds, TPI
 381 then determines the presence or absence of a streambed.

382



383

384 **Figure 4** : Classification trees to detect the presence of streambeds according to variables



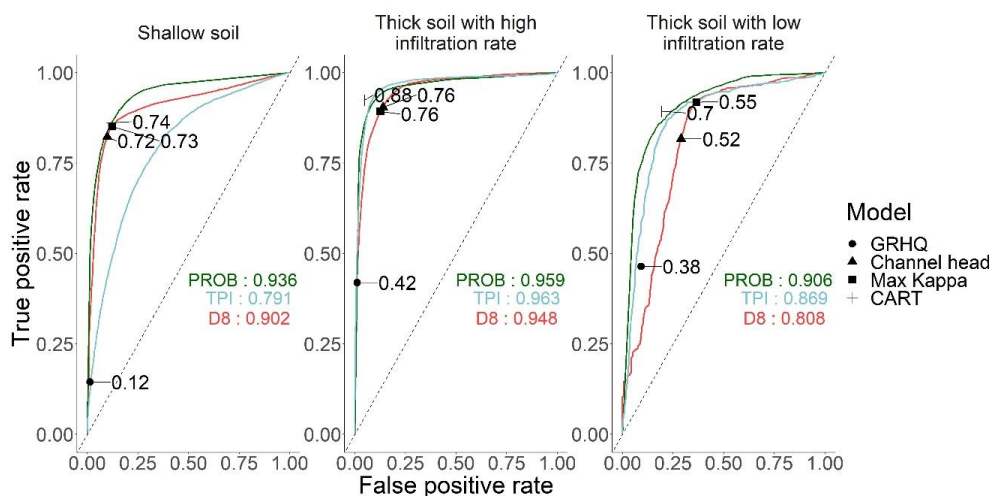
385 D8, PROB and TPI and hydrological class. **[Color is not required for this figure. 2**
386 **column fitting figure.]**

387

388 Figure 5 compares the AUC of individual variables, thus their potential to detect a
389 streambed. The performance of the four streambed models is also presented. This figure
390 shows that for the three hydrological classes, PROB performs more effectively than D8
391 when it comes to detecting streambeds. For thick soil classes, the incision variable TPI has
392 a higher AUC than D8. For shallow soil, the opposite is true. Compared to the other models,
393 the GRHQ has a very low true positive rate, meaning it omits many streams regardless of
394 the hydrologic class. However, the performance of GRHQ is higher for thick soils than for
395 shallow soils. For shallow soils, although the false positive rate is slightly lower for D8
396 thresholded with channel heads (Channel head), the Cohen's kappa of the classification
397 tree (CART) is still higher. The performance of the maximum Kappa of D8 (Max Kappa)
398 is still very similar to the one of the classification tree (CART). Figure 5 also shows that
399 the performance of the classification tree (CART) for shallow soil is not in the upper left
400 part of the ROC curve of the variable PROB. This observation is consistent with the fact
401 that only this variable was used to calibrate this model. Nevertheless, for both thick soil
402 classes, the performance of the classification trees (CART) is in the upper left part of the
403 ROC curve of the variable PROB. This means that the addition of the incision variable TPI
404 improves the detection of streambeds. For thick soils with high infiltration rates, the two
405 thresholding methods (Channel head and Max Kappa) yielded similar performances,
406 although they did not perform as well as the classification tree (CART). The performance
407 of the classification tree (CART) is also higher than both D8 thresholding methods for thick
408 soils with low infiltration rates. However, the method using the maximum Kappa (Max



409 Kappa) yields a higher rate of true positives than the thresholding method using the channel
 410 heads (Channel head).
 411



412
 413 **Figure 5** : ROC curve and AUC values from the logistic regressions of the three variables
 414 according to hydrological class. The performance of the streambed models using Cohen’s
 415 kappa is also presented. [Figure 5 about here. Color is not required for this figure. 2
 416 column fitting figure.]

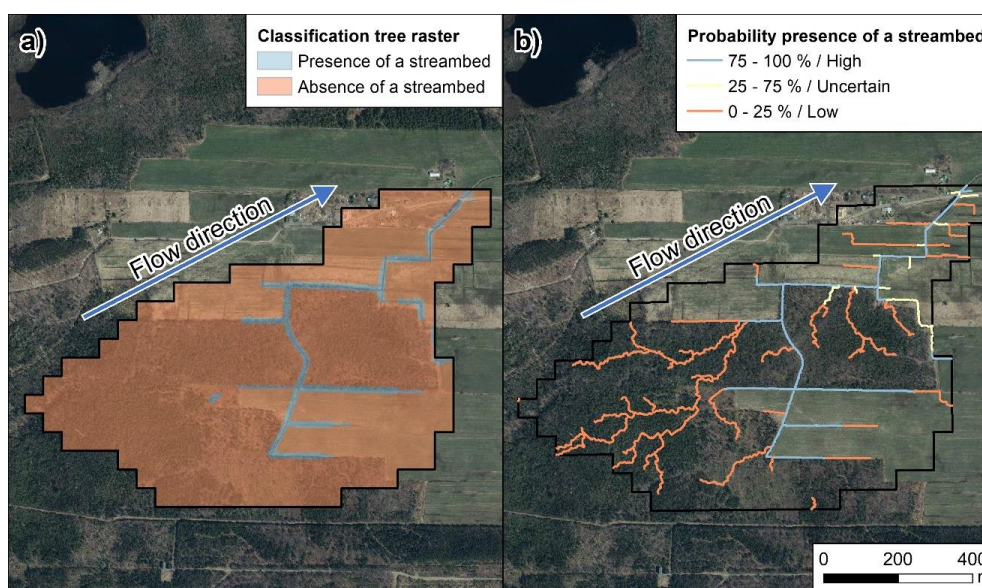
417

418 **5. Discussion**

419 The results suggest that the classification tree can detect streambeds more accurately than
 420 the other methods tested. By integrating different topographic indices and ground
 421 information such as surface deposits, the detection of headwater streambeds is much more
 422 efficient in large watersheds, despite the high anthropization of the ground that is
 423 sometimes present. In addition, as the results of the classification trees are rasters (Fig. 6
 424 a)), they can be easily integrated within attribute table of a drainage network by calculating



425 the mean using a zonal statistic to assess the probability presence of a streambed (Fig. 6
426 b)). This integration can be done without altering the course or thresholds of the
427 hydrographic network. Each segment can therefore be truncated according to the presence
428 or absence of the stream predicted by the model.
429



430

431

432 **Figure 6** : Classification tree that has been integrated into the segments of a hydrographic
433 network to assess the probability presence of a streambed (b) (Aerial images from
434 continuous imagery of the Government of Quebec; MRNF). [Color is not required for
435 this figure. 1.5 column fitting figure.]

436

437 The classification tree (CART) drastically increases the true positive rate compared to the
438 GRHQ. This is because the GRHQ was based on aerial photographs that were primarily
439 used to characterize vegetation and forest structure. Photointerpretation of these images



440 did not allow for the detection of streambeds formed by local fluvial processes under the
441 forest cover (Lessard, 2020). At most, photointerpretation enables the identification of
442 valleys, for example, on thick soils (Montgomery and Dietrich, 1994). For this reason, the
443 GRHQ omits fewer streams in thick soil than in shallow soil.

444 The PROB variable improved the detection of streambeds compared to the conventional
445 use of only the D8 variable, since it has been thresholded to accurately match the lowest
446 drainage areas of the channel heads. According to Fig. 3, the 1.5 ha threshold accounts for
447 the majority of the channel heads. However, the drainage areas of the channel heads are
448 generally higher for thick soils with low infiltration rates. The majority of the surveyed
449 streams in this hydrologic class are located in the Abitibi Lowlands natural province. Some
450 of the drainage areas of the channel heads in shallow soil are smaller than 1.5 ha.

451 For the shallow soil hydrological class, the PROB variable improves streambed detection
452 only when a false positive rate of at least 0.12 is specified. Figure 5 shows that for a false
453 positive rate of 0.25, for example, PROB has a higher true positive rate than the D8
454 variable. Streambeds that were not omitted with a PROB threshold greater than 0.12 were
455 mostly small streams with highly variable positions due to the slightly upstream convex
456 topography (Hengl et al., 2010). It seems that these streambed presence positions have very
457 low PROB values (48% of these positions have a probability below the 0.33 threshold used;
458 Fig. 4). The 0.33 PROB threshold enabled a false positive rate that is much lower than
459 0.25. In fact, the false positive rate was only 0.12. With this 0.33 threshold, the performance
460 of PROB was almost identical to D8. This is indicated on the figure by the two ROC curves
461 that were at their closest to each other at approximately the same place as the classification
462 tree model (CART) (Fig. 5). In order to increase the true positive rate while using the PROB



463 variable, the threshold could be decreased to allow the smallest streams to be identified.

464 However, this modification would increase the false positive rate.

465 The poor performance of the TPI variable for shallow soil is due to the fact that the surface
466 deposits are generally thin and the slopes are frequently steep. The ground is therefore less
467 prone to erosion and incision than for the other two hydrological classes (Jensen et al.,
468 2018; Montgomery and Dietrich, 1994). Indeed, the parameters used to compute TPI do
469 not enable the detection of small streambeds if they are not located in a valley or in a larger
470 incision. Furthermore, the hydrological processes involved in this class are mostly surface
471 flow and not subsurface flow. It is for this reason that D8 and PROB, which tend to be able
472 to quite precisely recreate surface flow, are the best performing variables in this
473 hydrological class (Julian et al., 2012; Wohl, 2018).

474 The incision variable TPI performed better in thick soils with high infiltration rates. This
475 seems to be due to the fact that unlike shallow soils which are generally thin, infiltrative
476 soils are thick and unconsolidated. Thus, the main hydrological process for this
477 hydrological class is a subsurface process, where the water table plays an important role in
478 the initiation of streambeds. Water infiltrates vertically into the permeable surface deposits
479 and recharges the groundwater (Dunne and Black, 1970). The locations of the channel
480 heads do not correspond to specific drainage areas that can be identified by flow
481 accumulation variables, but rather to local incisions formed by gully processes where
482 groundwater intersects the ground surface (Dietrich and Dunne, 1993; Wohl, 2018). This
483 process occurs where there is a significant change in slope or soil permeability. The
484 emergence of water from the ground leads to progressive gully processes that can be detected by
485 incision variables (Montgomery and Dietrich, 1994). In this context, groundwater depth



486 variables such as depth-to-water (DTW; (White et al., 2012)) could be used to explain the
487 presence of streams in areas where a water table is present. It is important to mention that
488 the DTW is very sensitive to parameterization and more research is needed for its proper
489 use (Drolet, 2020).

490 Streambeds were better detected using solely PROB instead of D8 for thick soils with low
491 infiltration rates, which occur in territories where there is a high proportion of wetlands
492 and gentle slopes. The PROB variable mostly reduces the number of commission cases.
493 For example, in Fig. 5, PROB had a much lower false positive rate than D8 for the same
494 true positive rate of 0.75. This large reduction in the false positive rate achieved with PROB
495 reflects the ability of this variable to reproduce a diffuse flow on very flat or slightly convex
496 terrains (Hengl et al., 2010). Indeed, in 78 % of cases, the positions that correspond to an
497 absence of a streambed and that are corrected with PROB are wetlands. This is noteworthy
498 because wetlands represent only 64 % of these positions in this hydrological class. Thus
499 the PROB variable, using uncertain DEM elevation information, can recreate more realistic
500 behavior of the water, especially in thick soils with low infiltration rates. By using both
501 PROB and TPI variables (Fig. 4), streambed detection for this hydrological class can be
502 improved compared to the use of a single variable. Because the deposits are unconsolidated
503 and the ground can be incised (Dietrich and Dunne, 1993), the classification tree is in the
504 upper left part of the ROC curve for the PROB variable as well as for the hydrological class
505 with the high infiltration. The use of the TPI variable therefore provides an advantage.
506 A limitation of the classification tree method is that the surface deposit mapping is not
507 accurate enough for all local hydrological issues. A visual inspection revealed some
508 inconsistencies in the surface deposit mapping within the same hydrological class.



509 Another limitation is associated with the anthropization and linearization of natural
510 streams. While a streambed is the result of a natural fluvial formation process that leads to
511 ground erosion, an anthropogenic ditch is an artificial bed that is formed by mechanized
512 digging. However, it is common for naturally formed streambeds to have been excavated
513 and linearized in agricultural areas. In these cases, it becomes very difficult to distinguish
514 a streambed from an anthropogenic ditch, even in the field. Excavation concentrates the
515 flow of water in the artificial bed (Moussa et al., 2002). Thus, an area with previously no
516 water flow could now be considered a stream (Roelens et al., 2018). Automated detection
517 methods are therefore likely to be much less reliable in these situations.

518 We believe that the method described for calibrating the classification tree model is simple
519 and robust enough to be applied in a different climatic and geomorphic context with local
520 data describing headwater streambeds. An accurate LiDAR derived headwater streambed
521 mapping is a powerful tool for government and local organizations involved in water
522 management and protection.

523

524 **6. Conclusion**

525 The classification tree method presented in this paper has improved the detection of
526 headwater streambeds for different hydrological contexts over large watersheds. Reliable
527 and consistent results were obtained by developing a comprehensive field database. The
528 variable PROB, which describes the probability of occurrence of a streambed, was used to
529 correct errors associated with the positioning of streambeds. This variable allowed for
530 marginal corrections of streambeds in shallow soil, particularly when a high threshold was
531 used. In order to more precisely explain where streams initiate in shallow soil, variables



532 characterizing the composition of the upstream watershed such as the average upstream
533 slope or the composition of deposits should be explored. The variable TPI, which
534 characterized small-scale incisions, significantly improved the detection of streambeds in
535 both thick soil hydrological classes when combined with the PROB variable. The small-
536 scale incision variable worked better in soils with high infiltration rates and the probability
537 of occurrence worked better in soils with low infiltration rates.

538 The increased complexity of the methods (inputs and parameterization) makes the
539 optimizations more difficult for very large territories. It is difficult to integrate the influence
540 of all physiographic variables into a single model and improvements require multiple
541 iterations which leads to high complexity. The integration of case studies could improve
542 models by directly focusing on some of the identified limitations. It is also important to
543 consider that the input data may sometimes be unreliable, such as those for the road
544 network, culverts, surface deposits and land use. Thus, developments, such as those
545 integrating surface deposits, will not be improve if the quality of the raw data remains
546 unchanged. Visual interpretation of map products and verification by an expert with a good
547 knowledge of the area is an essential step that should not be neglected under any
548 circumstances.

549

550 **Author contribution**

551 Francis Lessard and Naïm Perreault contributed to the research project by providing
552 expertise in methodology, software development, formal analysis, investigation, data
553 curation, writing, and visualization. Their contributions encompassed various stages, from
554 data collection and analysis to manuscript preparation.



555

556 Sylvain Jutras supervised the project, provided conceptual guidance, and played a role in
557 writing and reviewing the manuscript. Additionally, Jutras secured funding for the project
558 and managed administrative tasks related to its execution.

559

560 **Competing interest**

561 The authors declare that they have no conflict of interest.

562

563 **Acknowledgements**

564 The authors thank Quebec's Ministère de l'Environnement et de la Lutte contre les
565 changements climatiques (MELCC) and Ministère des Forêts, de la Faune et des Parcs
566 (MFFP), which funded this research project. This project would not have been possible
567 without the exceptional collaboration of the MELCC's and MFFP's LiDAR mapping
568 team, together with the many students and research associates who contributed to the
569 numerous field surveys.

570

571 **Data Availability**

572 Data and code can be found at https://github.com/FraLessard/headwater_streambeds.git,
573 hosted at GitHub (Lessard and Perreault, 2022).

574

575 **References**

576 Alexander, R. B., Boyer, E. W., Smith, R. A., Schwarz, G. E., Moore, R. B.: The role of
577 headwater streams in downstream water quality. *Journal of the American Water*



- 578 Resources Association, 43(1), 41–59. <https://doi.org/10.1111/j.1752->
579 [1688.2007.00005.x](https://doi.org/10.1111/j.1752-1688.2007.00005.x), 2007.
- 580 Band, L. E.: Topographic Partition of Watersheds with Digital Elevation Models. Water
581 Resources Research, 22(1), 15–24. <https://doi.org/10.1029/WR022i001p00015>,
582 1986.
- 583 Blouin, J., and Berger, J.-P. : Guide de reconnaissance des types écologiques de la région
584 écologique 5a – Plaine de l’Abitibi. Ministère des Ressources naturelles du Québec,
585 Forêt Québec, Direction des inventaires forestiers, Division de la classification
586 écologique et productivité des stations. 180 pp., 2002.
- 587 Blouin, J., and Berger, J.-P. : Guide de reconnaissance des types écologiques des régions
588 écologiques 5e – Massif du lac Jacques-Cartier et 5f – Massif du mont Valin.
589 Ministère des Ressources naturelles, de la Faune et des Parcs, Forêt Québec,
590 Direction des inventaires forestiers, Division de la classification écologique et
591 productivité des stations. 194 pp., 2004.
- 592 Breiman, L., Friedman, J. H., Olshen, R. A., & Stone, C. J.: Classification And Regression
593 Trees. Routledge. <https://doi.org/10.1201/9781315139470>, 1984.
- 594 Cho, H. C., Clint Slatton, K., Cheung, S., & Hwang, S.: Stream detection for LiDAR digital
595 elevation models from a forested area. International Journal of Remote Sensing,
596 32(16), 4695–4721. <https://doi.org/10.1080/01431161.2010.484822>, 2011.
- 597 Cohen, J.: A Coefficient of Agreement for Nominal Scales. Educational and Psychological
598 Measurement, 20(1), 37–46. <https://doi.org/10.1177/001316446002000104>, 1960.
- 599 Conrad, O., Bechtel, B., Bock, M., Dietrich, H., Fischer, E., Gerlitz, L., Wehberg, J.,
600 Wichmann, V., & Böhner, J.: System for Automated Geoscientific Analyses



- 601 (SAGA) v. 2.1.4. Geoscientific Model Development, 8(7), 1991–2007.
602 <https://doi.org/10.5194/gmd-8-1991-2015>, 2015.
- 603 Creed, I. F., Lane, C. R., Serran, J. N., Alexander, L. C., Basu, N. B., Calhoun, A. J. K.,
604 Christensen, J. R., Cohen, M. J., Craft, C., D’Amico, E., De Keyser, E., Fowler, L.,
605 Golden, H. E., Jawitz, J. W., Kalla, P., Katherine Kirkman, L., Lang, M. W.,
606 Leibowitz, S. G., Lewis, D. B., Marton, J., McLaughlin, D. L., Raanan-Kiperwas
607 H., Rains M. C., Rains K. C., Smith, L.: Enhancing protection for vulnerable
608 waters. Nature Geoscience, 10(11), 809–815. <https://doi.org/10.1038/NGEO3041>,
609 2017.
- 610 Dietrich, W. E., and Dunne, T.: Sediment budget for a small catchment in mountainous
611 terrain. Z. Geomorph. N. F., Suppl. Bd., 29, 191–206., 1978.
- 612 Dietrich, W. E., and Dunne, T.: The Channel head. In: Beven K. and Kirkby M.J., Eds.,
613 Channel Network Hydrology, Wiley, New York, 175-219., 1993.
- 614 Direction de l’expertise en biodiversité: Guide d’utilisation du Cadre écologique de
615 référence du Québec (CERQ). Ministère du Développement durable, de
616 l’Environnement et de la Lutte contre les changements climatiques (MDDELCC),
617 Québec. 24 pp., 2018.
- 618 Drolet, E. : Identification des zones de contrainte de drainage aux opérations forestières à
619 l’aide des données lidar. Master thesis. Department of Wood and Forest Science.
620 Université Laval. 62 pp., 2020.
- 621 Dunne, T., and Black, R. D.: An Experimental Investigation Runoff Production in
622 Permeable Soils. Water Resources Research, 6(2), 478–490.
623 <https://doi.org/10.1029/WR006i002p00478>, 1970.



- 624 Elmore, A. J., Julian, J. P., Guinn, S. M., & Fitzpatrick, M. C.: Potential Stream Density in
625 Mid-Atlantic U.S. Watersheds. PLoS ONE, 8(8), e74819.
626 <https://doi.org/10.1371/journal.pone.0074819>, 2013.
- 627 Estrada, D.: Smart Device / GNSS Receiver Assessment Study for Hydrographic. Office
628 of the State Engineer Information Technology Services Bureau GIS (OSE GIS). 48
629 pp., 2017.
- 630 Fairfield, J., and Leymarie, P.: Drainage Networks From Grid Digital Elevation Models.
631 Water Resources Research, 27(5), 709-717. <https://doi.org/10.1029/90WR02658>,
632 1991.
- 633 Fawcett, T.: An introduction to ROC analysis. Pattern Recognition Letters, 27(8), 861–
634 874. <https://doi.org/10.1016/j.patrec.2005.10.010>, 2006.
- 635 Freeman, M. C., Pringle, C. M., & Jackson, C. R.: Hydrologic connectivity and the
636 contribution of stream headwaters to ecological integrity at regional scales. Journal
637 of the American Water Resources Association, 43(1), 5–14.
638 <https://doi.org/10.1111/j.1752-1688.2007.00002.x>, 2007.
- 639 Fürnkranz, J.: Pruning Algorithms for Rule Learning. Machine Learning, 27, 139–172.
640 <https://doi.org/10.1023/A:1007329424533>, 1997.
- 641 Gosselin, J.: Guide de reconnaissance des types écologiques des régions écologiques 3a –
642 Collines de l’Outaouais et du Témiscamingue et 3b – Collines du lac Nominique.
643 Ministère des Ressources naturelles du Québec, Forêt Québec, Direction des
644 inventaires forestiers, Division de la classification écologique et de la productivité
645 des stations. 188 pp., 2002.
- 646 Gosselin, J.: Guide de reconnaissance des types écologiques de la région écologique 3d -



- 647 Coteaux des basses Appalaches. Ministère des Ressources naturelles et de la Faune,
648 Direction des inventaires forestiers, Division de la classification écologique et
649 productivité des stations. 186 pp., 2005a.
- 650 Gosselin, J.: Guides de reconnaissance des types écologiques de la région écologique 2b -
651 Plaine du Saint-Laurent. Ministère des Ressources naturelles et de la Faune,
652 Direction des inventaires forestiers, Division de la classification écologique et
653 productivité des stations. 188 pp., 2005b.
- 654 Goulden, T., Hopkinson, C., Jamieson, R., and Sterling, S.: Sensitivity of watershed
655 attributes to spatial resolution and interpolation method of LiDAR DEMs in three
656 distinct landscapes. *Water Resources Research*, 50(3), 1908-1927.
657 <https://doi.org/10.1002/2013WR013846>, 2014.
- 658 Guisan, A., Weiss, S. B., and Weiss, A. D.: GLM versus CCA spatial modeling of plant
659 species distribution. *Plant Ecology*, 143(1), 107–122.
660 <https://doi.org/10.1023/A:1009841519580>, 1999.
- 661 Heine, R. A., Lant, C. L., and Sengupta, R. R.: Development and comparison of approaches
662 for automated mapping of stream channel networks. *Annals of the Association of
663 American Geographers*, 94(3), 477–490. [https://doi.org/10.1111/j.1467-
664 8306.2004.00409.x](https://doi.org/10.1111/j.1467-8306.2004.00409.x), 2004.
- 665 Hengl, T., Heuvelink, G. B. M. M., and Van Loon, E. E.: On the uncertainty of stream
666 networks derived from elevation data: the error propagation approach. *Hydrology
667 and Earth System Sciences*, 14(7), 1153–1165. [https://doi.org/10.5194/hess-14-
668 1153-2010](https://doi.org/10.5194/hess-14-1153-2010), 2010.
- 669 Henkle, J. E., Wohl, E., and Beckman, N.: Locations of channel heads in the semiarid



- 670 Colorado Front Range, USA. *Geomorphology*, 129(3–4), 309–319.
671 <https://doi.org/10.1016/j.geomorph.2011.02.026>, 2011.
- 672 Horton, B. Y. R. E.: Erosional development of streams and their drainage basins;
673 Hydrophysical approach to quantitative morphology. *GSA Bulletin*, 56(3), 275–
674 370. [https://doi.org/10.1130/0016-7606\(1945\)56\[275:EDOSAT\]2.0.CO;2](https://doi.org/10.1130/0016-7606(1945)56[275:EDOSAT]2.0.CO;2), 1945.
- 675 James, L. A., Hunt, K. J., Winter, S. W., James, L. A., and Hunt, K. J.: The LiDAR-side of
676 Headwater Streams: Mapping Channel Networks with High-resolution
677 Topographic Data. *Southeastern Geographer*, 50(4), 523–539.
678 <https://doi.org/10.1353/sgo.2010.0009>, 2010.
- 679 James, L. A., Watson, D. G., and Hansen, W. F.: Using LiDAR data to map gullies and
680 headwater streams under forest canopy: South Carolina, USA. *Catena*, 71(1), 132–
681 144. <https://doi.org/10.1016/j.catena.2006.10.010>, 2007.
- 682 Jensen, C. K., McGuire, K. J., McLaughlin, D. L., and Scott, D. T.: Quantifying
683 spatiotemporal variation in headwater stream length using flow intermittency
684 sensors. *Environmental Monitoring and Assessment*, 191, 226.
685 <https://doi.org/10.1007/s10661-019-7373-8>, 2019.
- 686 Jensen, C. K., McGuire, K. J., Shao, Y., and Andrew Dolloff, C.: Modeling wet headwater
687 stream networks across multiple flow conditions in the Appalachian Highlands.
688 *Earth Surface Processes and Landforms*, 43(13), 2762–2778.
689 <https://doi.org/10.1002/esp.4431>, 2018.
- 690 Jenson, S. K., and Dominque, J. O.: Extracting topographic structure from digital elevation
691 data for geographic information system analysis. *Photogrammetric Engineering*
692 *and Remote Sensing*, 54(11), 1593–1600. 1988.



- 693 Julian, J. P., Elmore, A. J., and Guinn, S. M.: Channel head locations in forested watersheds
694 across the mid-Atlantic United States: A physiographic analysis. *Geomorphology*,
695 177–178, 194–203. <https://doi.org/10.1016/j.geomorph.2012.07.029>, 2012.
- 696 Leboeuf, A., and Pomerleau, I.: Projet d’acquisition de données par le capteur LiDAR à
697 l’échelle provinciale : analyse des retombées et recommandations. Ministère des
698 Forêts, de la Faune et des Parcs, Direction des inventaires forestiers. 15 pp., 2015.
- 699 Leopold, L. B., Wolman, M. G., and Miller, J. P.: *Fluvial Processes in Geomorphology*.
700 San Francisco, California, W. H. Freeman and Company, 522 pp., 1964.
- 701 Lessard, F. Optimisation cartographique de l’hydrographie linéaire fine. Master thesis.
702 Department of Wood and Forest Science. Université Laval. 89 pp., 2020.
- 703 Lessard, F., Jutras, S., Perreault, N., and Guilbert, E.: Performance of automated
704 geoprocessing methods for culvert detection in remote forest environments.
705 *Canadian Water Resources Journal*,
706 <https://doi.org/10.1080/07011784.2022.2160660>, 2023.
- 707 Li, R., Tang, Z., Li, X., and Winter, J. Drainage Structure Datasets and Effects on LiDAR-
708 Derived Surface Flow Modeling. *ISPRS International Journal of Geo-Information*,
709 2(4), 1136–1152. <https://doi.org/10.3390/ijgi2041136>, 2013.
- 710 Lindsay, J. B.: Sensitivity of channel mapping techniques to uncertainty in digital elevation
711 data. *International Journal of Geographical Information Science*, 20(6), 669–692.
712 <https://doi.org/10.1080/13658810600661433>, 2006.
- 713 Lindsay, J. B.: « Whitebox GAT: A Case Study in Geomorphometric Analysis ». *Computers
714 and Geosciences* 95: 75-84.
715 <https://doi.org/10.1016/j.cageo.2016.07.003>, 2016a.



- 716 Lindsay, J. B.: Efficient hybrid breaching-filling sink removal methods for flow path
717 enforcement in digital elevation models. *Hydrological Processes*, 30(6), 846-857.
718 <https://doi.org/10.1002/hyp.10648>, 2016b.
- 719 Lindsay, J. B., and Dhun, K.: Modelling surface drainage patterns in altered landscapes
720 using LiDAR. *International Journal of Geographical Information Science*, 29(3),
721 397–411. <https://doi.org/10.1080/13658816.2014.975715>, 2015.
- 722 Meyer, J. L., Strayer, D. L., Wallace, J. B., Eggert, S. L., Helfman, G. S., and Leonard, N.
723 E.: The contribution of headwater streams to biodiversity in river networks. *Journal*
724 *of the American Water Resources Association*, 43(1), 86–103.
725 <https://doi.org/10.1111/j.1752-1688.2007.00008.x>, 2007.
- 726 Ministère de l'Environnement et de la Lutte contre les changements climatiques
727 (MELCC): Normales climatiques du Québec 1981-2010. [data set].
728 <https://www.environnement.gouv.qc.ca/climat/normales/>, 2022.
- 729 Montgomery, D. R., and Dietrich, W. E.: Channel Initiation and the Problem of Landscape
730 Scale. *Science*, 255(5046), 826–830.
731 <https://doi.org/10.1126/science.255.5046.826>, 1992.
- 732 Montgomery, D. R., and Dietrich, W. E.: Landscape dissection and drainage area-slope
733 thresholds. In: Kirkby, M.J. (Ed.), *Process Models and Theoretical*
734 *Geomorphology*. John Wiley and Sons, 221–246. 1994.
- 735 Montgomery, D. R., and Foufoula-Georgiou, E.: Channel Network Source Representation
736 Using Digital Elevation Models. *Water Resources Research*, 29(12), 3925–3934.
737 <https://doi.org/10.1029/93WR02463>, 1993.
- 738 Moussa, R., Voltz, M., and Andrieux, P.: Effects of the spatial organization of agricultural



739 management on the hydrological behaviour of a farmed catchment during flood
740 events. *Hydrological Processes*, 16(2), 393–412. <https://doi.org/10.1002/hyp.333>,
741 2002.

742 Murphy, P. N. C., Ogilvie, J., Meng, F.-R. R., and Arp, P. A.: Stream network modelling
743 using lidar and photogrammetric digital elevation models: a comparison and field
744 verification. *Hydrological Processes*, 22(12), 1747–1754.
745 <https://doi.org/10.1002/hyp.6770>, 2008.

746 O’Callaghan, J. F., and Mark, D. M.: The extraction of drainage networks from digital
747 elevation data. *Computer Vision, Graphics, and Image Processing*, 28(3), 323–344.
748 [https://doi.org/10.1016/S0734-189X\(84\)80011-0](https://doi.org/10.1016/S0734-189X(84)80011-0), 1984.

749 O’Neil, G., and Shortridge, A.: Quantifying local flow direction uncertainty. *International*
750 *Journal of Geographical Information Science*, 27(7), 1292–1311.
751 <https://doi.org/10.1080/13658816.2012.719627>, 2013

752 Passalacqua, P., Belmont, P., and Foufoula-Georgiou, E.: Automatic geomorphic feature
753 extraction from lidar in flat and engineered landscapes. *Water Resources Research*,
754 48(3), 1–18. <https://doi.org/10.1029/2011WR010958>, 2012.

755 Persendt, F. C., and Gomez, C.: Assessment of drainage network extractions in a low-relief
756 area of the Cuvelai Basin (Namibia) from multiple sources: LiDAR, topographic
757 maps, and digital aerial orthophotographs. *Geomorphology*, 260, 32–50.
758 <https://doi.org/10.1016/j.geomorph.2015.06.047>, 2016.

759 Peucker, T. K., and Douglas, D. H.: Detection of Surface-Specific Points by Local Parallel
760 Processing of Discrete Terrain Elevation Data. *Computer Graphics and Image*
761 *Processing*, 4(4), 375–387. [https://doi.org/10.1016/0146-664x\(75\)90005-2](https://doi.org/10.1016/0146-664x(75)90005-2), 1975.



- 762 Roelens, J., Rosier, I., Dondeyne, S., Van Orshoven, J., and Diels, J.: Extracting drainage
763 networks and their connectivity using LiDAR data. *Hydrological Processes*, 32(8),
764 1026–1037. <https://doi.org/10.1002/hyp.11472>, 2018.
- 765 Saucier, J.-P., Berger, J.-P., D’Avignon, H., and Racine, P.: Le point d’observation
766 écologique. Ministère des Ressources naturelles, Direction de la gestion des stocks
767 forestiers, Service des inventaires forestiers. 116 pp., 1994.
- 768 Schwanghart, W., and Heckmann, T.: Fuzzy delineation of drainage basins through
769 probabilistic interpretation of diverging flow algorithms. *Environmental Modelling*
770 *and Software*, 33, 106–113. <https://doi.org/10.1016/j.envsoft.2012.01.016>, 2012.
- 771 St-Hilaire, A., Duchesne, S., and Rousseau, A. N.: Floods and water quality in Canada: A
772 review of the interactions with urbanization, agriculture and forestry. *Canadian*
773 *Water Resources Journal*, 41(1–2), 273–287.
774 <https://doi.org/10.1080/07011784.2015.1010181>, 2016.
- 775 Tribe, A.: Automated recognition of valley lines and drainage networks from grid digital
776 elevation models: a review and a new method. *Journal of Hydrology*, 139(1–4),
777 263–293. [https://doi.org/10.1016/0022-1694\(92\)90206-B](https://doi.org/10.1016/0022-1694(92)90206-B), 1992.
- 778 Tucker, G. E., and Slingerland, R.: Predicting sediment flux from fold and thrust belts.
779 *Basin Research*, 8(3), 329–349. <https://doi.org/10.1046/j.1365-2117.1996.00238.x>,
780 1996.
- 781 Van Meerveld, H. J. I., Kirchner, J. W., Vis, M. J. P., Assendelft, R. S., and Seibert, J.:
782 Expansion and contraction of the flowing stream network changes hillslope
783 flowpath lengths and the shape of the travel time distribution. *Hydrology and Earth*
784 *System Sciences*, 23(11), 4825–4834. <https://doi.org/10.5194/hess-23-4825-2019>,



- 785 2019.
- 786 Wechsler, S. P.: Uncertainties associated with digital elevation models for hydrologic
787 applications: a review. *Hydrology and Earth System Sciences*, 11(4), 1481–1500.
788 <https://doi.org/10.5194/hess-11-1481-2007>, 2007.
- 789 Weiss, A.: Topographic position and landforms analysis. Poster Presentation, ESRI User
790 Conference, San Diego, California. USA. 2001.
- 791 White, B., Ogilvie, J., Campbell, D. M. H., Hiltz, D., Gauthier, B., Chisholm, H. K. H.,
792 Wen, H. K., Murphy, P. N. C., and Arp, P. A.: Using the Cartographic Depth-to-
793 Water Index to Locate Small Streams and Associated Wet Areas across
794 Landscapes. *Canadian Water Resources Journal*, 37(4), 333–347.
795 <https://doi.org/10.4296/cwrj2011-909>, 2012.
- 796 Wohl, E.: The challenges of channel heads. *Earth-Science Reviews*, 185, 649–664.
797 <https://doi.org/10.1016/j.earscirev.2018.07.008>, 2018.
- 798 Wu, J., Liu, H., Wang, Z., Ye, L., Li, M., Peng, Y., Zhang, C., and Zhou, H.: Channel head
799 extraction based on fuzzy unsupervised machine learning method. *Geomorphology*,
800 391, 107888. <https://doi.org/10.1016/j.geomorph.2021.107888>, 2021.
- 801 Wulder, M. A., Bater, C. W., Coops, N. C., Hilker, T., White, J. C.: The role of LiDAR in
802 sustainable forest management. *Forestry Chronicle*, 84(6), 807–826.
803 <https://doi.org/10.5558/tfc84807-6>, 2008.